Ferroelectric Supercapacitors by Combining Polarization Switching and Negative Capacitance Effects for On-Chip Energy Storage

Sadegh Kamaei, Michele Ghini, Ali Gilani, Carlotta Gastaldi, Eloi Collette, and Adrian Mihai Ionescu, *Fellow, IEEE*

***Abstract*— In this work, we investigate the fundamental effects contributing to energy storage enhancement in on-chip ferroelectric electrostatic supercapacitors with doped high-k dielectrics. By optimizing energy storage density and efficiency in nanometer-thin stacks of Si:HfO_2 and Al_2O_3, we achieve energy storage density of 90 J/cm^3 with efficiencies up to 90%. We demonstrate for the first time that in such ferroelectric stacks, both negative capacitance and dipole switching contribute to energy density enhancement, with an enhancement of more than 30% when the negative capacitance regime is exploited. These findings lay the groundwork for the design and operation in the most appropriate regime of on-chip energy storage rechargeable devices based on ferroelectric stacks.**

***Index Terms*— Negative capacitance, ferroelectric materials, energy storage, NC supercapacitors.**

I. Introduction

As THE demand for autonomous Edge Artificial Intelligence and Internet-of-Things (IoT) systems grows, two major challenges have emerged: the need for electronics with improved energy efficiency and the possibility of eliminating batteries through integrated energy storage devices [1], [2]. Electrostatic solid-state supercapacitors based on polarized materials, such as ferroelectric (FE), have gained attention due to their potential for enhanced energy and power density [3], [4], [5]. Recently, negative capacitance (NC) has emerged as a potential solution for low-power transistor devices and capacitance charge boosting [6], [7], [8], [9], [10]. In 2019, Hoffman et al. proposed using NC to increase energy storage in electrostatic capacitors beyond conventional limits by incorporating a FE material into a linear dielectric (DE) capacitor [11]. However, the contributions of polarization charge and NC effects in FE-DE capacitors remain up to date unexplored. Additionally, exploring these effects in other doped hafnia FE materials can enable further optimization routes. Our study addresses these gaps by investigating the enhancement arising from polarization charge and decoupling it from the NC effect through short (500 ns) and long (1.5 ms) pulse measurements on a silicon-doped hafnia (Si:HfO_2)-Al_2O_3 stack with polarized and non-polarized FE layers. We also examine the effect of the DE-to-FE thickness ratio on energy storage density and enhancement. Our findings show high efficiency (90%), energy storage density (90 J/cm^3), and more than 30% enhancement in stored energy density when the NC region is exploited.

Manuscript received 20 June 2023; revised 10 July 2023; accepted 16 July 2023. Date of publication 19 July 2023; date of current version 25 August 2023. This work was supported by the advanced European Research Council (ERC) grant "N Supercap" under Grant ID: 966786. The review of this letter was arranged by Editor M. H. Park. *(Sadegh Kamaei and Michele Ghini contributed equally to this work.)* *(Corresponding author: Sadegh Kamaei.)*

The authors are with the Nanoelectronic Devices Laboratory, École Polytechnique Fédérale de Lausanne (EPFL), 1015 Lausanne, Switzerland (e-mail: sadegh.kamaeibahmaei@epfl.ch).

Color versions of one or more figures in this letter are available at https://doi.org/10.1109/LED.2023.3296945.

Digital Object Identifier 10.1109/LED.2023.3296945

II. Principle and Fabrication Process

We conducted a qualitative analysis to understand how NC in ferroelectric can be utilized to create a capacitor with considerably higher energy densities than a capacitor without an NC layer (Fig. 1). We examined the behavior of the FE-DE stack in three distinct regimes: FE-DE stack with inactive FE layer (case 1), displaying a linear charge-voltage (Q-V) behavior; FE-DE stack with activated FE layer, exhibiting nonlinearity due to spontaneous polarization (case 2); and activated FE layer with NC effect (case 3). In case (2), operational parameters prevent exploiting the NC region, ensuring that the observed behavior is only attributed to polarization switching rather than the NC effect. By comparing cases (2) and (3), we can determine the contribution of the NC effect and polarization charge to the observed increase in energy storage density. Notably, in cases (1) and (2) the stacks behave like two positive capacitors in series, leading to lower energy density than the dielectric alone. On the other hand, the NC supercapacitor in case (3) displays enhanced energy storage without hysteresis losses.

To study the above-mentioned cases, we fabricated FE-DE capacitors using Si:HfO_2 and dielectric Al_2O_3 thin films. A fabricating process begins with a p-doped Si wafer covered by 100 nm SiO_2 to avoid interference from the Si substrate. A bottom electrode of 4 nm/40 nm Ti/Pt is deposited using an evaporation and lift-off process. Next, a 10 nm thick TiN layer is sputtered, followed by the atomic layer deposition (ALD) of a 10.5 nm Si:HfO_2 film. The ALD deposition is performed at 300 °C using TEMA-Hf and $SiH_2(N(C_2H_5)_2)_2$ (SAM24) as precursors, with water and ozone used as oxygen sources. A second 12 nm thick TiN layer is deposited, and a rapid thermal annealing process (RTA) is performed at 600 °C for 2 minutes in nitrogen to activate ferroelectricity, except

This work is licensed under a Creative Commons Attribution-NonCommercial-NoDerivatives 4.0 License.
For more information, see https://creativecommons.org/licenses/by-nc-nd/4.0/

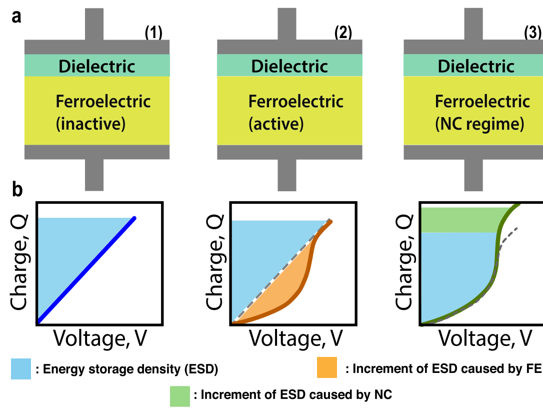

Fig. 1. Schematic of the FE-DE capacitors (a) and their related energy storage densities (b) in the three regimes considered.

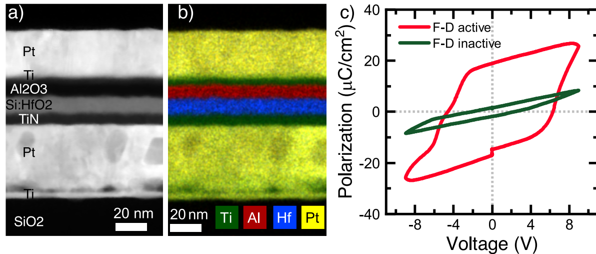

Fig. 2. a) High-angle annular dark-field STEM and b) EDS elemental composition mapping of a typical device cross-section. c) P-V hysteretic loops of two representative FE-DE devices, with and without activated ferroelectricity.

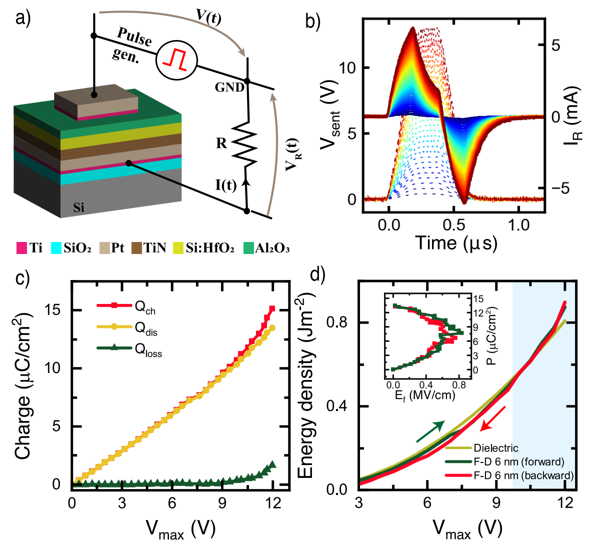

Fig. 3. a) Illustration of the experimental setup. b) Applied pulses and the corresponding current across R. c) Calculated Q-V behavior of the capacitor up to the breakdown voltage (12.5 V). d) Comparison of discharge energy density for DE layer vs. FE-DE device in a double-sweep experiment, showing energy enhancement in NC regime with no hysteresis losses. Inset: P-E_f curves obtained by increasing and decreasing applied potential.

for samples with an inactive ferroelectric layer. In all active ferroelectric samples, the desired orthorhombic crystalline phase and a 3.4% Si doping concentration were successfully obtained, consistent with our previous study [12]. The top TiN layer is then etched away using a wet etch process [13]. Next, various thicknesses of Al_2O_3 are deposited on the stack by varying the number of ALD cycles. Capacitors with an area of 10^4 μm^2 are defined by the evaporation of 4 nm/30 nm Ti/Pt followed by a lift-off step. A similar process is used to fabricate TiN/Al_2O_3/Ti/Pt reference capacitors to obtain the permittivity of the Al_2O_3 layer. Given the scalability and CMOS compatibility of the proposed fabrication process, such NC supercapacitors can be integrated on the back of the chip in the near future, a solution aligned with the current trend of having buried power lines [14], [15]. Moreover, the device's compact footprint allows for seamless integration into space-limited IoT nodes without compromising the form factor.

A cross-sectional scanning transmission electron microscopy (STEM) image of a representative capacitor and its corresponding energy dispersive spectroscopy (EDS) analysis are shown in Figs 2a and 2b. The accurate thickness, uniform deposition, and material composition of each layer in the stack can be observed. Fig. 2c shows the P-V results obtained on the samples comprising 6 nm thick Al_2O_3 (labeled as F-D 6nm) with and without an activated FE layer. The obtained P-V loops demonstrate the RTA process induces ferroelectricity, while the inactive sample behaves similarly to a linear DE.

III. Results and Discussion

A. Si:HfO_2-Al_2O_3 NC Supercapacitors

Pulsed charge-voltage measurements were performed to experimentally validate the presence of NC effect and the energy behavior in the proposed Si:HfO_2/Al_2O_3 capacitors [12], [16]. Fig. 3a-c shows the experimental setup, the applied short pulse waveform with the measured current during the capacitor's charging/discharging, and the calculated Q-V curves for the charging (Q_{ch}), discharging (Q_{dis}), and their difference (Q_{loss}). In Fig 3d, we compare the discharge energy density per unit area of the F-D 6nm capacitor with the calculated density of the Al_2O_3 layer alone. The energy density of the DE (W_D) was calculated based on its measured permittivity ($\sim$ 7) and the W_D = 1/2 CV^2 formula, while the values of the FE-DE capacitor were obtained experimentally from the integrated charges during discharging by using the formula $W = \int_0^Q V dQ$. The energy enhancement originates from the exploitation of non-linear Q-V behavior under the hysteresis-free NC regime. These results show that in the NC regime (blue region) the discharge energy density curve of the FE-DE stack dominates over the DE alone. Furthermore, there is no hysteresis between increasing and decreasing applied pulses as the ferroelectric enters the NC region of the "S"-shaped P-E curve for both sweep directions (inset of Fig 3d), demonstrating the fulfillment of the capacitance matching condition of both layers.

The impact of the DE-to-FE thickness ratio on energy storage enhancement and density is also examined by varying the DE thickness from 6 to 10 nm. Fig. 4a shows the evolution of the energy enhancement factor with changing DE thickness. According to the known formula for energy enhancement in NC supercapacitors [11], $W/W_D \approx 1$ - aC, where perfect matching occurs at (aC = -1) [17]. Here, C represents the capacitor. In a series combination of a negative and a positive capacitor, the W/W_D ratio can exceed one, contrary to what occurs in a classical series combination of positive capacitors where the total capacitance is always reduced. Hence, the stabilization and matching of NC are crucial for achieving enhancement values greater than one. The obtained value of 1.1 (aC $= -0.11$) for the 6 nm Al_2O_3 sample indicates suboptimal capacitance matching. In contrast, the samples with 8 and 10 nm thick DE layers show higher energy

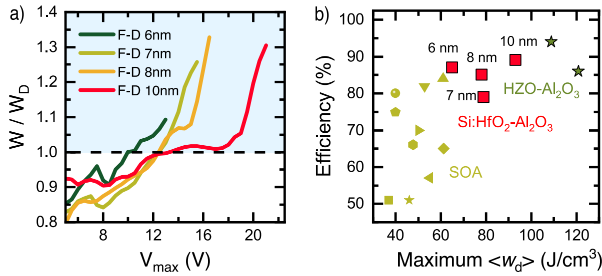

Fig. 4. a) NC energy density enhancement (W/W_D) for all investigated FE-DE devices. b) Comparison of efficiency and maximum energy density between solid-state supercapacitors, FE-DE supercapacitors based on HZO, and Si:HfO_2 (this work). SOA values are from [11].

enhancement values up to 1.31 (aC = −0.31), indicating better matching conditions. Fig. 4b compares the energy density and efficiency values obtained from the investigated stacks with those reported for electrostatic supercapacitors made from non-epitaxial materials. The Si:HfO_2-based NC supercapacitor exhibits exceptional performance surpassing previous reports and comparable values to a similar stack made of HZO film. Incrementing the thickness of the Al_2O_3 layer up to 10 nm led to values of 93 J/cm^3 for the maximum energy density with an efficiency of 90%. Overall, increasing the DE-to-FE ratio improves the capacitor's energy density, but can decrease voltage gain due to reduced capacitance matching. Thus, there is an optimal DE layer thickness, where the impact on both capacitance matching and energy density is balanced.

B. Exploiting the Combined Effects of Polarization Switching and Negative Capacitance

In order to evaluate the impact of polarization switching on the FE-DE stack, we employed long-pulsed measurements on two sets of structurally identical samples (F-D 6nm and F-D 10nm) with and without activated ferroelectricity. All samples were made on the same wafer under identical conditions to minimize fabrication process variations. This ensures consistency among the samples, including the crystalline phase of the Si:HfO_2 in activated samples. Long pulses of 1.5 ms were used to ensure that NC effects do not affect the discharge dynamics of the capacitors. By fitting the discharge currents with a simple exponential function, we obtained the discharge capacitance values for both sets of samples, as shown in Fig. 5a. These capacitance values, depicted in Fig. 5b, allowed us to quantify the enhancement in equivalent capacitance induced by the formation of polarization domains as a function of applied voltage. The ratio of the capacitance values obtained from the active FE samples to their inactive counterparts ($C/C_{inactive}$) indicates a 15% and 25% enhancement due to the activation of the FE layer in F-D 10nm and F-D 6nm, respectively. Notably, when the thickness ratio of DE-to-FE increases, the impact of FE polarization switching becomes less significant. This is because the majority of the energy is stored in the DE layer and as the thickness of this layer increases the effect of dipole switching decreases. In fact, the total energy is mainly due to the DE layer, and the difference between active and inactive stacks becomes smaller as the thickness of the DE layer increases when the capacitor is operated in a non-NC regime.

By normalizing the energy density functions of both the isolated DE layer and of the FE-DE stack with activated

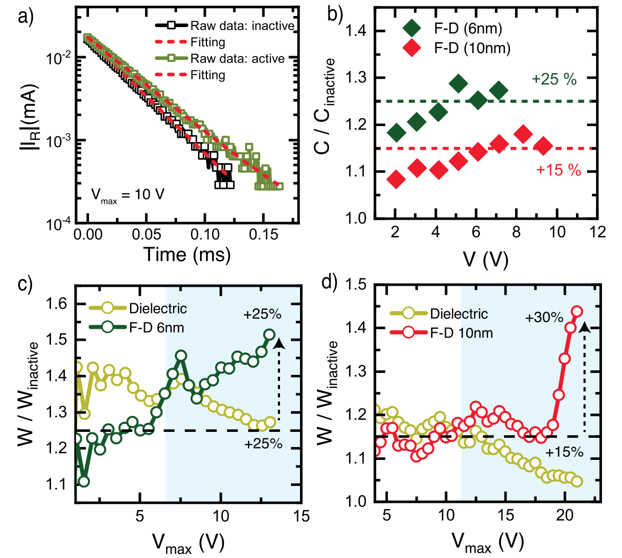

Fig. 5. a) Discharge current and fits in F-D 10nm samples with and without activated ferroelectricity at V_{max} = 10V. b) Capacitance enhancement ratio vs. applied voltage for F-D 6nm (10nm) sample, showing a 25% (15%) increase due to polarization switching. (c, d) Energy density comparison of activated Si:HfO_2/Al_2O_3 capacitor vs. dielectric layer alone, normalized to inactive FE sample based on short pulse experiment data. Results show 25% (15%) polarization switching impact and an additional 25% (30%) negative capacitance (blue area), consistent with the long pulse experiment data in (b).

ferroelectricity against the inactive FE-DE capacitor ($W/W_{inactive}$), it is possible to identify and decouple the impact of polarization domains and negative capacitance. Short pulse experiments were used to obtain energy density values of the active and inactive samples, while the DE data points were calculated based on its permittivity. As shown in Figs. 5c, 5d, the energy density enhancement in the samples with 6 and 10 nm DE layer was 15% and 25%, respectively, when the FE was activated, which is consistent with the data obtained from long-pulse measurements (Fig. 4b). However, an additional 30% and 25% enhancement is attributed to the realization of NC in the stacks. The region in which the stack operates in the NC regime coincides with the part of the curve where the energy density of the FE-DE stack outperforms that of the DE alone.

IV. Conclusion

We conducted an experimental study to explore how polarization switching and the NC effect of FE contribute to the energy storage density of FE-DE capacitor structures. By performing short and long-pulse experiments on two identical samples, one with activated ferroelectric and one without, we were able to isolate the effects of polarization switching and NC. Our study found that matching the capacitances of the FE and DE layers, achieved in this case by increasing the thickness of the Al_2O_3 layer, can significantly enhance energy storage. We obtained discharged energy densities of over 90 J/cm^3 with efficiencies exceeding 90%. Further improvements in the quantitative enhancement are expected by using linear 2D dielectrics with higher permittivity. These results open the way to the development of advanced solid-state supercapacitors that enable highly efficient short-term energy storage through careful analysis of polarization switching and capacitance matching.

References

[1] A. M. Ionescu, "Energy efficient computing and sensing in the zettabyte era: From silicon to the cloud," in *IEDM Tech. Dig.*, Dec. 2017, pp. 1–2, doi: 10.1109/IEDM.2017.8268307.

[2] C. Lethien, J. Le Bideau, and T. Brousse, "Challenges and prospects of 3D micro-supercapacitors for powering the Internet of Things," *Energy Environ. Sci.*, vol. 12, no. 1, pp. 96–115, 2019, doi: 10.1039/C8EE02029A.

[3] M. H. Park, H. J. Kim, Y. J. Kim, T. Moon, K. D. Kim, and C. S. Hwang, "Thin $Hf_xZr_{1-x}O_2$ films: A new lead-free system for electrostatic supercapacitors with large energy storage density and robust thermal stability," *Adv. Energy Mater.*, vol. 4, no. 16, Nov. 2014, Art. no. 1400610, doi: 10.1002/aenm.201400610.

[4] B. Peng, Q. Zhang, X. Li, T. Sun, H. Fan, S. Ke, M. Ye, Y. Wang, W. Lu, H. Niu, J. F. Scott, X. Zeng, and H. Huang, "Giant electric energy density in epitaxial lead-free thin films with coexistence of ferroelectrics and antiferroelectrics," *Adv. Electron. Mater.*, vol. 1, no. 5, May 2015, Art. no. 1500052, doi: 10.1002/aelm.201500052.

[5] A. Chauhan, S. Patel, R. Vaish, and C. Bowen, "Anti-ferroelectric ceramics for high energy density capacitors," *Materials*, vol. 8, no. 12, pp. 8009–8031, Nov. 2015, doi: 10.3390/ma8125439.

[6] J. Li, J. Zhou, G. Han, Y. Liu, Y. Peng, J. Zhang, Q.-Q. Sun, D. W. Zhang, and Y. Hao, "Negative capacitance Ge PFETs for performance improvement: Impact of thickness of $HfZrO_x$," *IEEE Trans. Electron Devices*, vol. 65, no. 3, pp. 1217–1222, Mar. 2018, doi: 10.1109/TED.2018.2791420.

[7] J. Zhou, G. Han, N. Xu, J. Li, Y. Peng, Y. Liu, J. Zhang, Q.-Q. Sun, D. W. Zhang, and Y. Hao, "Incomplete dipoles flipping produced near hysteresis-free negative capacitance transistors," *IEEE Electron Device Lett.*, vol. 40, no. 2, pp. 329–332, Feb. 2019, doi: 10.1109/LED.2018.2886426.

[8] C. Jin, T. Saraya, T. Hiramoto, and M. Kobayashi, "On the physical mechanism of transient negative capacitance effect in deep subthreshold region," *IEEE J. Electron Devices Soc.*, vol. 7, pp. 368–374, 2019, doi: 10.1109/JEDS.2019.2899727.

[9] K. D. Kim, Y. J. Kim, M. H. Park, H. W. Park, Y. J. Kwon, Y. B. Lee, H. J. Kim, T. Moon, Y. H. Lee, S. D. Hyun, B. S. Kim, and C. S. Hwang, "Transient negative capacitance effect in atomic-layer-deposited $Al_2O_3/Hf_{0.3}Zr_{0.7}O_2$ bilayer thin film," *Adv. Funct. Mater.*, vol. 29, no. 17, Apr. 2019, Art. no. 1808228, doi: 10.1002/adfm.201808228.

[10] M. Hoffmann, B. Max, T. Mittmann, U. Schroeder, S. Slesazeck, and T. Mikolajick, "Demonstration of high-speed hysteresis-free negative capacitance in ferroelectric $Hf_{0.5}Zr_{0.5}O_2$," in *IEDM Tech. Dig.*, Dec. 2018, pp. 31.6.1–31.6.4, doi: 10.1109/IEDM.2018.8614677.

[11] M. Hoffmann, F. P. G. Fengler, B. Max, U. Schroeder, S. Slesazeck, and T. Mikolajick, "Negative capacitance for electrostatic supercapacitors," *Adv. Energy Mater.*, vol. 9, no. 40, Oct. 2019, Art. no. 1901154, doi: 10.1002/aenm.201901154.

[12] C. Gastaldi, M. Cavalieri, A. Saeidi, E. O'Connor, F. Bellando, I. Stolichnov, and A. M. Ionescu, "Negative capacitance in HfO_2 gate stack structures with and without metal interlayer," *IEEE Trans. Electron Devices*, vol. 69, no. 5, pp. 2680–2685, May 2022, doi: 10.1109/TED.2022.3157579.

[13] S. Kamaei, A. Saeidi, C. Gastaldi, T. Rosca, L. Capua, M. Cavalieri, and A. M. Ionescu, "Gate energy efficiency and negative capacitance in ferroelectric 2D/2D TFET from cryogenic to high temperatures," *NPJ 2D Mater. Appl.*, vol. 5, no. 1, p. 76, Sep. 2021, doi: 10.1038/s41699-021-00257-6.

[14] A. Gupta, Z. Tao, D. Radisic, H. Mertens, O. V. Pedreira, S. Demuynck, J. Bömmels, K. Devriendt, N. Heylen, S. Wang, K. Kenis, L. Teugels, F. Sebaai, C. Lorant, N. Jourdan, B. T. Chan, S. Subramanian, F. Schleicher, A. Peter, N. Rassoul, Y. Siew, B. Briggs, D. Zhou, E. Rosseel, E. Capogreco, G. Mannaert, A. Sepúlveda, E. Dupuy, K. Vandersmissen, B. Chehab, G. Murdoch, E. A. Sanchez, S. Biesemans, Z. Tokei, E. D. Litta, and N. Horiguchi, "Buried power rail integration for CMOS scaling beyond the 3 nm node," *Proc. SPIE*, vol. 12056, 2022, Art. no. 120560B, doi: 10.1117/12.2615641.

[15] D. Prasad, S. S. T. Nibhanupudi, S. Das, O. Zografos, B. Chehab, S. Sarkar, R. Baert, A. Robinson, A. Gupta, A. Spessot, P. Debacker, D. Verkest, J. Kulkarni, B. Cline, and S. Sinha, "Buried power rails and back-side power grids: Arm CPU power delivery network design beyond 5nm," in *IEDM Tech. Dig.*, Dec. 2019, pp. 1–19, doi: 10.1109/IEDM19573.2019.8993617.

[16] M. Hoffmann, F. P. G. Fengler, M. Herzig, T. Mittmann, B. Max, U. Schroeder, R. Negrea, P. Lucian, S. Slesazeck, and T. Mikolajick, "Unveiling the double-well energy landscape in a ferroelectric layer," *Nature*, vol. 565, no. 7740, pp. 464–467, Jan. 2019, doi: 10.1038/s41586-018-0854-z.

[17] S. Salahuddin and S. Datta, "Use of negative capacitance to provide voltage amplification for low power nanoscale devices," *Nano Lett.*, vol. 8, no. 2, pp. 405–410, Feb. 2008, doi: 10.1021/nl071804g.